Development of a Land Surface Model Including Evaporation and Adsorption Processes in the Soil for the Land–Air Exchange in Arid Regions

GENKI KATATA AND HARUYASU NAGAI

Japan Atomic Energy Agency, Ibaraki, Japan

HIROMASA UEDA

Acid Deposition and Oxidant Research Center, Nigata, Japan

NURIT AGAM AND PEDRO R. BERLINER

Wyler Department for Dryland Agriculture, Jacob Blaustein Institute for Desert Research, Ben-Gurion University of the Negev, Sede Boqer, Israel

(Manuscript received 6 September 2006, in final form 23 February 2007)

ABSTRACT

A one-dimensional soil model has been developed to better predict heat and water exchanges in arid and semiarid regions. New schemes to calculate evaporation and adsorption in the soil were incorporated in the model. High performance of the model was confirmed by comparison of predicted surface fluxes, soil temperature, and volumetric soil water content with those measured in the Negev Desert, Israel. Evaporation and adsorption processes in the soil have a large impact on the heat and water exchange between the atmosphere and land surface and are necessary to accurately predict them.

Numerical experiments concerning the drying process of soil are performed using the presented model and a commonly used land surface model. The results indicated that, when the dry soil layer (DSL) develops, water vapor flux to the atmosphere is caused by evaporation in the soil rather than evaporation at the ground surface. Moreover, the adsorption process has some impact on the water and heat balance at the ground surface. The upward water vapor flux during the daytime is due to evaporation of soil water in the DSL, which is stored during the night due to adsorption. When the DSL progresses sufficiently, almost the same amounts of water are exchanged between the air and the soil surface by daytime evaporation and nighttime adsorption. In such conditions, latent heat due to evaporation and adsorption in the soil also work to reduce the diurnal variation of surface temperature.

1. Introduction

More than half of the land surface on the globe is arid or semiarid and many researchers have reported that desertification is increasing as a result of climate change (such as global warming) and human activities (e.g., Verstraete and Schwartz 1991; Puigdefabregas 1995; Warren 1996). At the same time, scarcity of water resources is of great concern in light of population growth and food shortages. Understanding the water cycle in arid and semiarid regions on the basis of heat and water exchanges between air and the soil surface is necessary to solve these problems.

In bare soil, evaporation at the soil–atmosphere interface is the dominant process for water vapor exchange during the daytime. When the soil is wet, evaporation at the soil surface contributes to changes in atmospheric conditions. The soil water at the interface evaporates due to radiative heating. When the soil is wet, liquid water is supplied from the underlying soil layer (USL) to the surface by capillary action. Under dry soil conditions, evaporation at the interface is inhibited as a result of a decrease in soil water supplied from the USL and a dry soil layer (DSL), in which soil water retained by adsorption forces forms a soil surface layer (Shimojima et al. 1990; Hillel 1998; Rose et al. 2005). In this case, soil water mainly evaporates at the

Corresponding author address: Genki Katata, Japan Atomic Energy Agency, 2-4 Shirakata-shirane, Tokai, Naka, Ibaraki, Japan.
E-mail: katata.genki@jaea.go.jp

DOI: 10.1175/2007JHM829.1

USL–DSL interface, and water vapor is diffused in the DSL and released into the atmosphere. During the night, when a gradient in water vapor directs the latent heat flux toward the soil surface, water vapor in the air deposits on the soil surface owing to condensation and adsorption processes. If the soil surface temperature is below the dewpoint, water vapor in the air condenses at the soil surface. Alternatively, when the soil temperature is higher than the dewpoint, water vapor in the air is adsorbed by the soil in the DSL. Water vapor adsorption in bare soil was found to be the most important water source in desert areas during the dry season [Agam (Ninari) and Berliner 2006]. The formation of DSL and the processes of evaporation, condensation, and adsorption in the soil, therefore, can play an important role in water exchange in arid environments.

Evaporation and adsorption are not only important for water exchange but mainly for energy exchange between the air and the soil surface. Latent heat due to phase changes affects the energy balance at the soil surface. The radiant energy partitioning at the land–air interface is described by an energy balance equation,

$$R_{\text{net}} = G + H + \text{lE}, \tag{1}$$

where R_{net} is the net radiation, and G, H, and lE are the soil and sensible and latent heat fluxes (W m^2 s^{-1}), respectively. However, lE above dry soil is much smaller than the other energy balance components. It is therefore commonly accepted in large-scale models that the lE above a dry soil is negligible and radiant energy is partitioned into H and G only (Cleugh and Roberts 1994; Unland et al. 1996). However, a recent study has found that lE above dry soil was not negligible, although a large fraction of the R_{net} was partitioned as H [Agam (Ninari) et al. 2004]. It has revealed that even when the water content of the topsoil is significantly lower than the wilting point, at which commonly used models would assume no latent heat flux, the value of lE was 20% of the R_{net} during the night and 10%–15% during the daytime. They concluded that models that assume no latent heat flux during the dry season may lead to erroneous results. It is also indicated that the lE due to evaporation and adsorption in the soil can have a strong effect on the heat budget at the soil surface in arid environments.

The processes of heat and water exchanges between the air and the soil surface play an important role in determining the global and regional meteorological conditions. Many land surface models have been developed during the last decade to describe the patterns of radiant energy partitioning at the air–land interface, as reviewed by Yang et al. (1998). For instance, a land surface model called the Noah Land Surface Model (LSM; Chen and Dudhia 2001a) was used as part of the fifth-generation Penn State–National Center for Atmospheric Research (NCAR) Mesoscale Model (MM5). Mesoscale models of this type were mainly developed for temperate climate zones (Bougeault 1991). Noah LSM has already been validated in several humid areas such as Kansas (Chen and Dudhia 2001b; Sridhar et al. 2002). However, when applying such models to arid climate regions several problems may emerge. First, these models assume no latent heat flux once the water content at the topsoil drops below the wilting point. Second, it is also assumed in these models that evaporation occurs only at the soil surface. Third, adsorption, which is a major process of water exchange at the air–land interface, is not included in the models. These problems probably have a less significant impact on the atmospheric field in temperate climates but are considered to be crucial in arid regions. A refined land surface model that includes these processes is, therefore, necessary to accurately consider heat and water exchanges at the air–land interface in arid environments.

A detailed one-dimensional model for atmosphere–soil–vegetation interaction called SOLVEG has been developed (Yamazawa and Nagai 1997; Nagai and Yamazawa 1999), and its performance has been examined for short vegetated areas (Nagai 2002, 2003, 2005). SOLVEG is unique in the way it treats the amount of evaporation (or condensation) in the soil to express the phase change process between liquid and water vapor in the soil. Many soil models have been developed based on the simultaneous transfer equations of heat and materials formulated by Philip and DeVries (1957; e.g., Grifoll et al. 2005). These kinds of models assume local thermodynamic equilibrium for liquid water and water vapor. Although theoretical analyses have shown that this assumption is valid under most natural conditions (Milly 1982), its limitations have not been discussed in terms of phase change process between liquid and water vapor. It is therefore important to investigate the assumption of thermodynamic equilibrium using a mechanistic model such as SOLVEG that includes phase change process. The formulation of the phase change process in SOLVEG must be modified and validated using detailed observed data of evaporation rate and soil water content. The objective of this study is to modify the SOLVEG formulation to calculate evaporation in the soil and incorporate the adsorption process into the soil component of SOLVEG for dry soil applications. Model calculations of soil temperature, soil moisture, and surface fluxes under dry soil conditions are compared to field measurements acquired at the Negev Desert, Israel, during the dry season. Numerical experiments using the modified SOLVEG

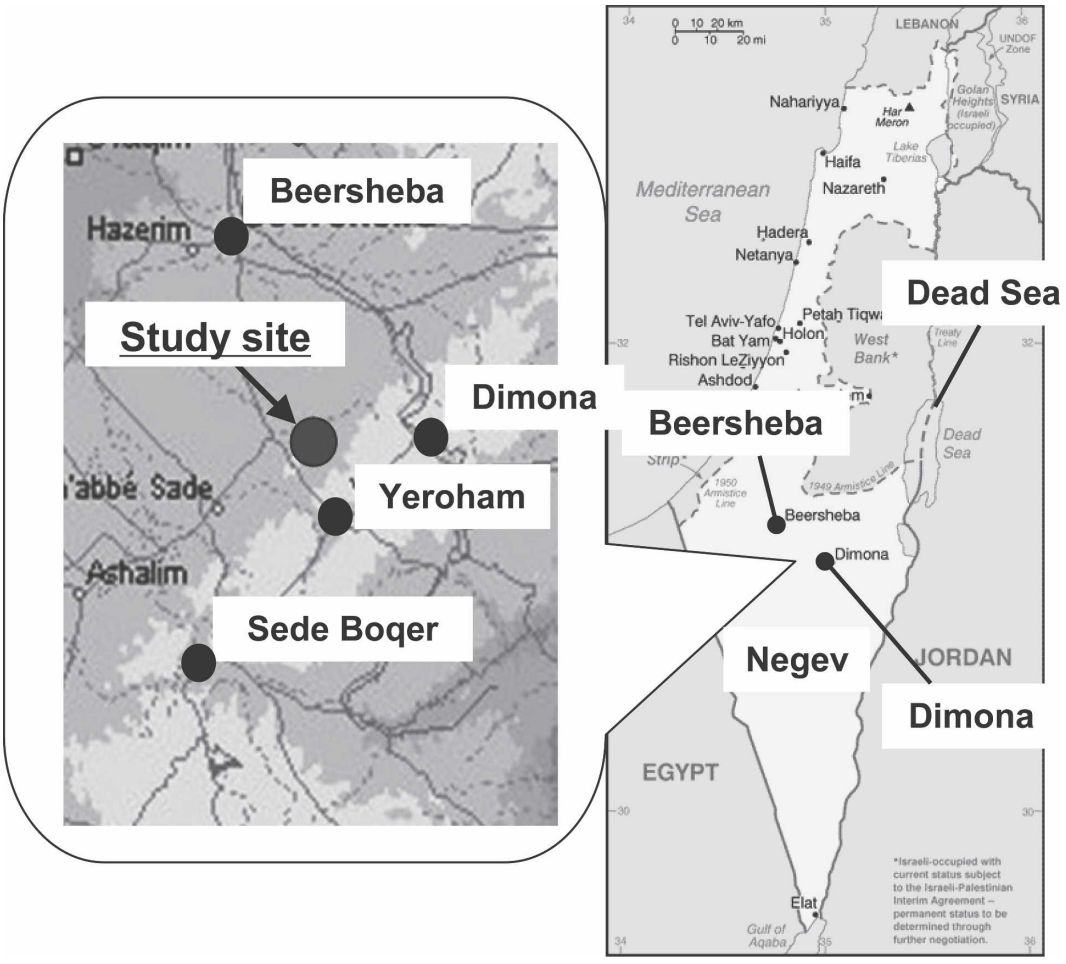

FIG. 1. Location of the study area in the Negev Desert, Israel.

(hereafter mod-SOLVEG) and Noah LSM were also performed to evaluate the effect of these processes on water and heat exchanges at the air–land interface.

2. Observed data

Data acquired at the Wadi Mashash Experimental Farm in the northern Negev are used in this study. The experimental farm is located at 31°08′N, 34°53′E, 400 m AMSL, 60 km from the Mediterranean Sea (Fig. 1). Micrometeorological data were collected during the dry season (from June to October) of 2002. Detailed site and observational descriptions can be found in Agam (Ninari) and Berliner (2004) and Agam (Ninari) et al. (2004).

A micrometeorological station was installed for continuous measurement of incoming and reflected shortwave radiation using two pyranometers (CM5, Kipp and Zonen); net radiation (Q-7, Campbell Scientific, Inc.); wind speed at four levels (2, 1, 0.5, and 0.25 m) with cup anemometers (014A Met-One); dry- and wet-bulb temperatures a height of 1 m using a self-designed aspirated psychrometer; soil heat flux at three different locations in the field with heat flux plates (HFT-3, Campbell Scientific, Inc.) installed at a depth of 50 mm; and temperature measurements above them at 10-mm intervals, using differentially wired thermocouples. Data were measured and collected every 10 s and averaged every 30 min by a datalogger (23X, Campbell Scientific, Inc.).

During nine 24-h field campaigns that took place during the experimental periods, sensible heat flux was measured with a sonic anemometer (CA27, Campbell Scientific, Inc.). Soil moisture content of the 100-mm uppermost soil layer was measured by hourly sampling and was determined in 10-mm increments. In addition, latent heat flux was derived from the changes in mass of an improved microlysimeter (Ninari and Berliner 2002) every half hour. The scale had a resolution of 0.1 g, which is equivalent to a resolution of 0.004 mm (equiva-

lent depth of water) or 5.11 W m^{-2} (in energy terms). The output of the scale was registered automatically every half hour by a palm computer (48GX, Hewlett Packard). In arid environments, small errors in the parameters used in micrometeorological methods (Brutsaert 1982) for the measurement of latent heat flux cause errors that are on the order of magnitude of the latent heat flux itself since the magnitude of the flux is very small (Ninari and Berliner 2002). However, direct methods using a microlysimeter theoretically provide an absolute reference for latent heat flux, as long as the soil heat balance in the microlysimeter is identical to that of the surrounding area. An analysis of thermal images of soil surface verified that the soil conditions in the microlysimeter were representative of the surrounding soil [Agam (Ninari) et al. 2004]. Moreover, when comparing the microlysimeter-derived latent heat fluxes to those computed from the soil moisture sampling, no systematic under- or overestimation was found [Agam (Ninari) and Beliner 2004]. The changes in soil water content measured by the microlysimeter are therefore reliable and representative of the changes in the soil water content (and thus the latent heat flux) of the surrounding soil.

To check the quality of the flux measurements the energy balance closure was examined. In the scatterplot of the sum of sensible and latent heat fluxes versus the sum of net radiation and soil heat flux, the regression line had a slope of 0.9 and a correlation coefficient of 0.93 [Agam (Ninari) et al. 2004]. These statistics indicate satisfactory closure.

3. Soil model

a. Basic equations

In the present study, the soil component of SOLVEG was modified. A detailed description of the model can be found in Nagai (2002). In mod-SOLVEG, the soil was divided into multiple layers and the set of equations for heat conduction, liquid, and water vapor transfers were numerically solved using an implicit finite-difference method and Gaussian elimination.

The temporal change in soil temperature is expressed by the heat conduction equation as

$$C_s\rho_s \frac{\partial T_s}{\partial t} = \frac{\partial}{\partial z}\left(\lambda \frac{\partial T_s}{\partial z}\right) - l\hat{E}_b, \tag{2}$$

where t is the time (s), z the depth of the soil (m), T_s the soil temperature (K), λ the thermal conductivity (W m^{-1} K^{-1}), l the latent heat of vaporization (J kg^{-1}), and $\hat{E}_b$ the phase changes of soil water (kg m^{-2} s^{-1}).

The mass balance equation for liquid water is given as

$$\rho_w \frac{\partial \eta_w}{\partial t} = \rho_w \frac{\partial}{\partial z}\left(D_w \frac{\partial \eta_w}{\partial z} + K\right) - \hat{E}_b, \tag{3}$$

where η_w is the volumetric soil water content (m^3 m^{-3}), D_w is the soil water diffusivity (m^2 s^{-1}), K is the unsaturated hydraulic conductivity (m s^{-1}), and ρ_w is the density of liquid water (kg m^{-3}). The soil water diffusivity D_w is expressed by

$$D_w = K\frac{\partial \psi}{\partial \eta_w}, \tag{4}$$

where ψ is the water potential (m).

Water vapor diffusion in the soil is considered in mod-SOLVEG; and according to Fick's law, the diffusion equation of water vapor in the soil pores is expressed as

$$\rho\frac{\partial(\eta_{ws} - \eta_w)q_s}{\partial t} = \frac{\partial}{\partial z}\rho\varepsilon\left[D_v(\eta_{ws} - \eta_w)\frac{\partial q_s}{\partial z}\right] + \hat{E}_b, \tag{5}$$

where q_s is the specific humidity in the soil pores (kg kg^{-1}), D_v is the diffusion coefficient of water vapor (m^2 s^{-1}), ε is the tortuosity (−), ρ is the density of water vapor (kg m^{-3}), and η_{ws} is the saturated volumetric water content (m^3 m^{-3}). The variable $(\eta_{ws} - \eta_w)$ represents the volumetric content of gaseous phase in the soil. Here, ε was chosen as two-thirds, as recommended by Jackson et al. (1974). Convection of water vapor is neglected in mod-SOLVEG because its contribution to water vapor transport near the soil surface is small under the natural condition that moderate heating and cooling processes are caused by diurnal change of solar radiation (Grifoll et al. 2005). Although empirical relations for the water vapor enhancement factor have been proposed to match measurements with predictions of the Philip and DeVries (1957) model, such modifications have not yielded satisfactory agreement with field data (De Vries 1987; Cahill and Parlange 1998). Mod-SOLVEG simulates water vapor movement in the soil without introducing such empirical relations.

b. Soil water retention curve

The soil water retention curve is essential for the simulation of liquid and water vapor flow in an unsaturated zone. SOLVEG uses the commonly employed curve suggested by Brooks and Corey (1964) and expressed as

$$\psi = \psi_s\left(\frac{\eta_w}{\eta_{ws}}\right)^{-b}, \tag{6}$$

$$\text{and} \quad K = K_s\left(\frac{\eta_w}{\eta_{ws}}\right)^{2b+3}, \tag{7}$$

where ψ_s and K_s are the saturated values of water potential (m) and K (m s^{-1}), respectively, and b is the empirical constant. These equations are widely used in various land surface models because of their simplicity. The function of Eq. (6) has, however, significant limitations at low soil water content. Since the Brooks and Corey's curve has been designed for wet soil, it is generally used to predict ψ when η_w is larger than the wilting point. The curve, hence, cannot be applied to dry soil. Moreover, water vapor adsorption is controlled by water retention curves in dry soil. The direct use of the curve for dry soil leads to errors not only in the prediction of the actual soil water content but also in the evaluation of adsorption processes in dry soil. An applicable curve for dry soil is therefore needed.

To avoid this problem, we adopted a modified soil water retention curve suggested by Webb (2000) consisting of two regions: the capillary region (Van Genuchten 1980) and the adsorption region (Campbell and Shiozawa 1992). The functions of both curves are described by Webb (2000) as

$$\psi = \begin{cases} \alpha^{-1}(S_w^{-(1/m)} - 1)^{(1/n)} & (\eta_w \geq \eta_{\mathrm{wm}}) \\ 10^{[\gamma(S - S_{wm}) + \log_{10}\psi_m]} & (\eta_w < \eta_{\mathrm{wm}}) \end{cases}, \quad S_w = (S - S_r)/(1 - S_r), \tag{8}$$

where S, S_r, S_w, and S_{wm} are the saturation ratio, residual and effective saturation ratio, and the corresponding value of S_w when $\eta_w = \eta_{\mathrm{wm}}$ (−), respectively; α, m, and n are fitting parameters (−); and ψ_m is water potential (m). The K can be described by combining Mualem's pore size distribution model (Mualem 1976).

The soil water retention curve [Eq. (8)] for Negev soil together with Eq. (6) for sandy loam soil (Cosby et al. 1984) are shown in Fig. 2a. The summary of soil parameters is listed in Table 1. As seen in Fig. 2a, the values of ψ calculated by Eq. (6) approach infinity with decreasing amounts of water in the dry soil. In contrast, the modified curves can be applied to the regions from water saturation to extreme drying.

c. Phase change processes of soil water

The processes of evaporation and adsorption in the soil play an important role in arid environments, as mentioned before. The explicit calculation of the evaporation process in the soil, $\hat{E}_b$, incorporated in SOLVEG is described by Eqs. (2), (3), and (5). We propose a new model for $\hat{E}_b$ and introduce it to the SOLVEG.

In mod-SOLVEG, the soil is formed by aggregation of "cylindrical pores," each of which have a different radius, as shown in Fig. 3a. We assume that only two patterns of pores exist. One is filled with capillary water, and the other is filled with air and adsorbs water on its wall. The drying mechanism of the soil in mod-SOLVEG is illustrated by Fig. 3b. When the soil is almost saturated, evaporation occurs at soil pores exposed to the air at the ground surface [direct evaporation, E_{dir} , defined later in Eq. (23)]. In this case, evaporation does not occur in the soil since almost all the pores are filled with capillary water (Fig. 3b, 1). When the soil dries out, pores with a large radius are dehydrated and adsorb water films on their walls. As a result, evaporation of water adsorbed by large pores [evaporation in the soil, $\hat{E}_b$ in Eqs. (2), (3), and (5)] contributes to the water vapor flux in addition to evaporation from small water-filled pores at the ground surface (Fig. 3b, 2). When the soil is extremely dry, all pores except for micropores are dehydrated and evaporation mainly occurs in the soil instead of at the ground surface (Fig. 3b, 3). In mod-SOLVEG, water vapor flux at the air–land interface (i.e., total evaporation at the soil surface; $z = 0$) represents the sum of direct evaporation (E_{dir}) and water vapor flux from the pores with adsorbed water film to the atmosphere [E_0 defined later in Eq. (26)], which results in evaporation in the soil throughout all soil layers. Similar models on the basis of cylindrical capillaries have been widely used to describe hydraulic and thermodynamic characteristics in unsaturated porous media (e.g., Mualem 1976). In the present study, we apply this concept to describe the phase change processes in the soil.

Considering the two patterns of pores (Fig. 3a), a threshold radius of pores, r_k (m), which determines whether a pore is filled with capillary water or not, is expressed as

$$r_k = \frac{2\tau \cos\phi}{\rho_w g \psi}, \tag{9}$$

where τ is the surface tension of the liquid water (=0.072) (N m^{-2}), ϕ is the contact angle of water (=0) (degree), and g is the gravity acceleration (m s^{-2}). The largest pore radius in the filled pores, r (m), is calcu-

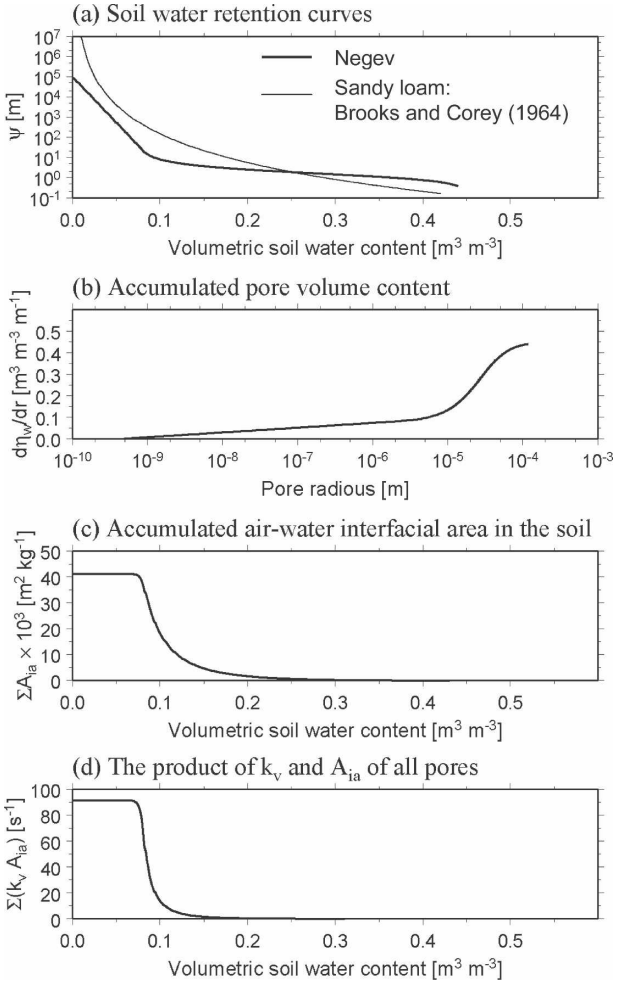

FIG. 2. (a) Soil water retention curves, (b) cumulative pore volume, (c) cumulative air–water interfacial area in the soil (A_{ia}), and (d) the product of mass transfer coefficient (k_v) and A_{ia} of all pores of Negev soil. The thin line in (a) represents the curve of sandy loam as referred to by Brooks and Corey (1964).

lated by $r = r_k + t$, where t is the film thickness of liquid water adsorbed on walls. Here, t is given by (Derjaguin et al. 1987; Iwamatsu and Horii 1996)

$$t = \sqrt[3]{\frac{A_{svl}}{6\pi\rho_w g\Pi}}, \tag{10}$$

where A_{svl} is the Hamaker constant (J) for solid–vapor interactions through an intervening liquid (for condensation $A_{svl} < 0$) and Π is the disjoining pressure (m). Or and Tuller (1999) determined $A_{svl} = -6.0 \times 10^{-20}$ (J) using soil data from Campbell and Shiozawa (1992). If interfacial interaction between the adsorbed water and the pore's wall surface is only induced by van der Waals forces, we can assume that the disjoining pressure Π is replaced by the water potential ψ (Tuller et al. 1999). It is assumed that only liquid film exists in the pores whose radius is larger than r_k. Using the soil water retention curve and the above formulations, we obtain the pore size distribution of the soil. The soil water retention curve and a distribution of cumulative pore volumes for the Negev soil are depicted in Figs. 2a and 2b, respectively. The cylindrical pore model detailed above has often been used to estimate pore size distribution of absorbents, for example, activated carbon and silica gel (Barrett et al. 1951; Wheeler 1955; Cranston and Inkley 1957; Dollimore and Heal 1964).

The liquid–vapor interfacial area in the soil [A_{ia} (m^2 m^{-3})] is simultaneously calculated with the discrete pore size distribution and is described as

$$A_{ia}(r) = 2\pi\kappa(r - t)L(r)\left(\sum_{r_{min}}^{r} A_{ia}(r) \le SA\right), \tag{11}$$

where κ is the fitting parameter (−), $L(r)$ is the pore length with r per unit volume (m m^{-3}), r_{min} is the minimum radius in all of pores (m), and SA is the specific

TABLE 1. Soil parameters for a determination of soil water retention curve of the Negev soil, where m_c is the clay content, η_{ws} is the saturated soil water content, ψ_s and b are the parameters for Brooks and Corey (1964), α and n are the parameters for Van Genuchten (1980), η_{wr} is the residual volumetric water content, and K_s is the saturated hydraulic conductivity. Single asterisk (*): used in Eq. (6). Double asterisk (**): used in Eqs. (6) and (8).

Name	Texture	m_c %	η_{ws} $m^{-3}m^{-3}$	ψ_s m	b*	α** m^{-1}	n**	η_{wr} $m^{-3}m^{-3}$	$K_s \times 10^{-5}$ m s^{-1}
Pacha[a]	Loam	8.5	0.430	—	—	0.682	2.10	0.0580	1.230[d]
Yolo[b]	Silt Loam	18.0	0.480	—	—	0.926	2.08	0.0850	1.230[d]
Noah LSM[c]	Sandy Loam	—	0.434	0.141	4.74	—	—	0.0470	0.523
Negev[d]	Sandy Loam	13.0	0.450	—	—	0.780	2.48	0.0750	1.230[d]

[a] Jackson (1964).
[b] Chen et al. (2000).
[c] Cosby et al.(1984).
[d] In this study.

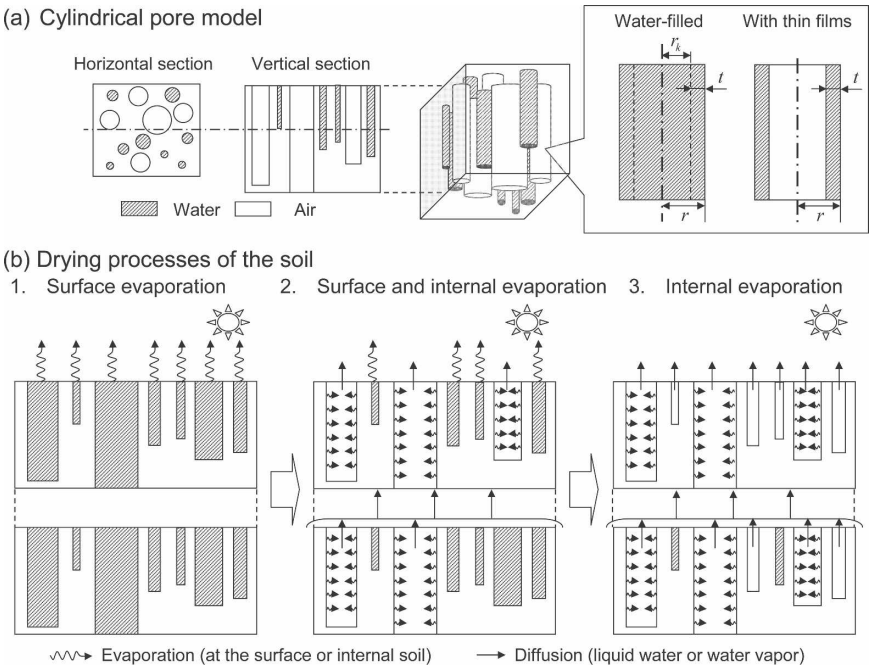

FIG. 3. Schematic diagrams of (a) the cylindrical pore model and (b) the drying process of soil due to evaporation at the ground surface or in the soil.

surface area ($m^2\ m^{-3}$). Here, κ is determined from the fact that cumulative A_{ia} does not exceed measured SA. From data from several soils (Petersen et al. 1996; Campbell and Shiozawa 1992; Banin and Amiel 1970), we obtained the following equation for SA:

$$SA = (0.06m_c^2 + 2.01m_c + 5.0) \times 10^3, \qquad (12)$$

where m_c is the clay content (%). The following function of lognormal pore radius distribution, $f(r) = d\eta_w/dr$, is used in this study (Kosugi 1994):

$$f(r) = \frac{\eta_{ws}}{(2\pi)^{1/2}\omega r} \exp\left\{-\frac{[\ln(r/r_m)]^2}{2\omega^2}\right\}, \qquad (13)$$

where r_m is the geometric mean radius (m), which is determined by ψ_{rm} (m) by (9), and ω is standard deviation (m). Here, ψ_{rm} and ω are obtained from van Genuchten's parameters of α and m

$$\psi_{rm} = -\alpha^{-1}(2^{1/m} - 1)^{1-m}, \qquad (14)$$

$$\text{and} \quad \omega^2 = (1 - m)\ln[(2^{1/m} - 1)/m]. \qquad (15)$$

Kosugi (1994) has reported that this model performs as well as any existing empirical model for determining retention curves of various soils. Using (13), $L(r)$ is expressed from the surface area of a cylindrical pore

$$L(r) = \frac{f(r)dr}{\pi r^2} \approx \frac{f(r)\Delta r}{\pi r^2}. \qquad (16)$$

Discrete calculation of $f(r)$ and $L(r)$ in the regions divided into 400 from water saturation to extreme drying is carried out at each pore radius.

Assuming that the distribution of the relative humidity of air adjacent to adsorbed water is similar in all pores, when the relative humidity of air adjacent to adsorbed water is smaller than 35%, almost all pores are filled with air and adsorb water according to the Brunauer–Emmett–Teller (BET) theory (Brunauer et al. 1938). Thus, we use the value of κ when the adsorbed water content, η_{wads}, is almost equal to η_w. The variable η_{wads} is described as

$$\eta_{wads} = \eta_w \frac{\sum_{r_{min}}^{r} A_{ia}(r)}{SA}. \qquad (17)$$

The capillary water content, η_{wmat}, is also determined as η_{wmat} ($= \eta_w - \eta_{wads}$). The changes of η_{wads} and η_{wmat} with ψ are shown in Fig. 4 a. A fitted value of $\kappa = 4.5 \times 10^{-6}$ was used in this study. Figure 2c shows a cumulative value of A_{ia} calculated by Eq. (11) for the Negev Desert. The general trend of A_{ia} is similar to results from other studies showing a large interfacial area at low saturation levels that gradually decreases with increasing saturation ratio (Reeves and Celia 1996; Kim et al. 1997; Tuller et al. 1999; Zand-Parsa and Sepaskhah 2004).

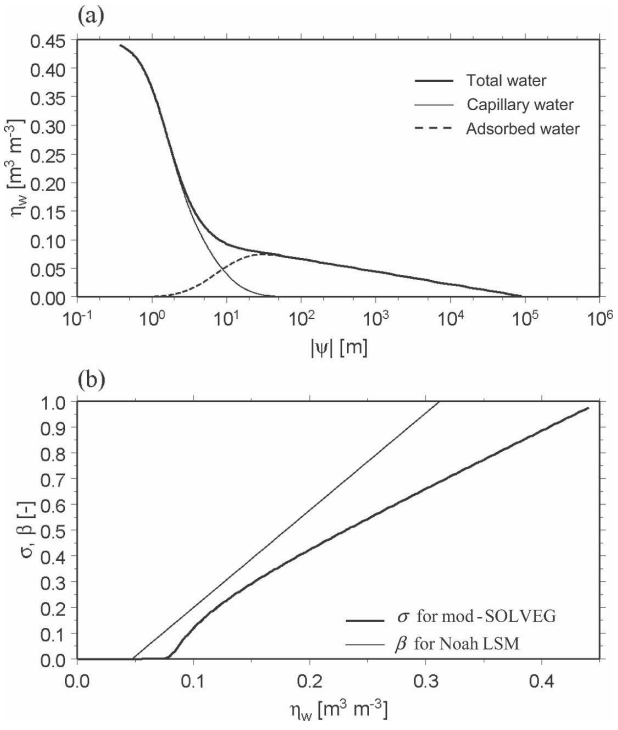

FIG. 4. (a) Adsorbed, capillary, and total water contents of the Negev soil (thick lines: total soil water content; thin lines: capillary water content; dashed lines: adsorbed water content) and (b) σ of mod-SOLVEG and β of the Noah LSM.

To describe the evaporation process in the soil, a mass transfer model in the cylindrical tube (Bird et al. 2001) was applied to mod-SOLVEG. Since we assumed that specific humidity of air adjacent to adsorbed water is equally distributed in all pores, the evaporation rate of adsorbed water in a pore with r, $\hat{E}_b(r)$, is determined by

$$\hat{E}_b(r) = \rho k_v(r) A_{\mathrm{ia}}(r)(q_{\mathrm{wall}} - q_s), \tag{18}$$

where $k_v(r)$ is the mass transfer coefficient (m s^{-1}) for a pore with r, q_{wall}, and q_s are the specific humidity at the surface of water adsorbed on the wall and at the center of the cylindrical pore, respectively. Coefficient k_v is calculated as follows:

$$k_v(r) = \frac{1.83 D_v}{r - t}, \tag{19}$$

where a value of 1.83 represents the Sherwood number of developed laminar flow of a circular tube (−). It can be assumed that the gaseous phase in the soil is quiescent or laminar if any flow exists under small difference in pressure between the atmosphere and the soil (Rolston 1986), and liquid–vapor interfaces remains stable (Ransohoff and Radke 1988; Blunt and Scher 1995). Under such condition, the mass transfer coefficient between the pore wall and bulk phase is constant (i.e., Sherwood number = 3.66) in the cylindrical tube regardless of bulk flow velocity if any; in other words, the mass transfer coefficient is proportional to inverse r. Thus, if pore size distribution in the soil is given, mod-SOLVEG can provide the amount of evaporation in the soil, which is an integrated value of $\hat{E}_b(r)$ throughout all pore radiuses. This is a new approach to describe detailed movements of liquid and water vapor including phase change processes in the soil.

In mod-SOLVEG, evaporation occurs in pores not filled with capillary water whose radius is larger than r_k as calculated by Eq. (9). Therefore, the total evaporation rate in the soil at a certain η_w is represented by

$$(k_v A_{\mathrm{ia}})_{\mathrm{tot}} = \int_{r_k}^{r_{\max}} k_v(r) A_{\mathrm{ia}}(r)\, dr \approx \sum_{r_k}^{r_{\max}} k_v(r) A_{\mathrm{ia}}(r) \Delta r, \tag{20}$$

where $r_{\max}$ is the maximum radius in all of the pores (m). The change of $(k_v A_{\mathrm{ia}})_{\mathrm{tot}}$ for η_w is shown in Fig. 2d. The result reveals the general concept of decreasing $(k_v A_{\mathrm{ia}})_{\mathrm{tot}}$ with a increase in soil water, which is similar to that reported by other experimental studies showing that nonaqueous phase liquids (NAPL) vapor phase mass transfer is inversely related to volumetric NAPL content (Anwar et al. 2003). This indicates that an increase of interfacial areas with a decrease in pores filled with capillary water allows more evaporation conductance of soil water; in other words, a thermodynamic equilibrium is formed between water vapor and liquid water when the soil dries out. This result is similar to previously reported theoretical analyses (Milly 1982).

The value q_{wall} is assumed to be equal to the specific humidity of air at the surface of liquid water adsorbed in the pores. When the soil water is in thermodynamic equilibrium, the relative humidity of the air adjacent to the adsorbed water in the pores, h_{ae}, is defined as (Israelachvili 1992)

$$h_{\mathrm{ae}} \equiv \exp\left(\frac{\psi g}{R_w T_s}\right), \tag{21}$$

where R_w is the gas constant of water vapor (J mol^{-1} K^{-1}); q_{wall} is thus expressed as

$$q_{\mathrm{wall}} = h_{\mathrm{ae}} q_{\mathrm{sat}}(T_s). \tag{22}$$

Equation (21), combined with Eq. (9), forms the Kelvin equation, which is widely used to calculate the vapor pressure in thermodynamic equilibrium within a Representative Elementary Volume (REV). It also provides the relation of capillary radius (r) and saturated vapor pressure (q_{wall}) on spherical meniscus of

TABLE 2. Comparisons of physical processes between mod-SOLVEG and Noah LSM.

Item	Modified SOLVEG	Noah LSM
Predicted variables	Soil temperature, volumetric water content, specific humidity in the soil pore	Soil temperature, volumetric water content
Evaporation at the ground	Included	Included (Mahfouf and Noilhan 1991)
Evaporation in the soil and adsorption	Included	Not included

the same curvature radius. Here, Kelvin's law is assumed to express vapor pressure of adsorbate on the cylindrical pore wall since it can be considered that vapor pressure of the water film adsorbed on the cylindrical pore wall with the same curvature radius, where van der Waals force works, is in the same order as that on the spherical meniscus. In mod-SOLVEG, the soil water potential expressed by Eq. (8), which includes these effects, is used to calculate ψ in Eq. (21) instead of Eq. (9).

Vapor diffusion with coefficient $(k_v A_{ia})_{tot}$ in Eq. (20) between the surface of adsorbed water and the air at the center of the cylindrical pore (evaporation or condensation in the soil) is caused by $q_{wall} - q_s$. The q_{wall} calculated by Eq. (22) rapidly decreases with decreasing soil water. When q_{wall} finally becomes q_s, evaporation (or condensation) in the soil by Eq. (18) stops.

We use the following equation for direct evaporation at the ground surface from the pores filled with capillary water, E_{dir}, which is regarded as evaporation:

$$E_{dir} = \rho\sigma c_{E0}|\mathbf{u}|[q_{sat}(T_{s0}) - q_r], \quad (23)$$

where σ is the fractional area of pores filled with capillary water exposed to the air ($\approx\eta_{wmat}/\eta_{ws}$) (−), c_{E0} is the bulk coefficient (−), $\mathbf{u}$ is the horizontal wind speed, T_{s0} is the soil surface temperature (°C), and q_r is the specific humidity of the air (kg kg^{-1}). The change of σ is shown in Fig. 4b. The area of σ becomes almost zero when $\eta = 0.08$ (m^3 m^{-3}); hence, we consider that there are almost no pores exposed to the air when η_w is less than 0.08. Considering the term E_{dir}, the upper boundary conditions are expressed as

$$-\left(D_w \frac{\partial \eta_w}{\partial z} + K\right)\bigg|_{z=0} = -P_r + E_r + E_{dir}, \quad (24)$$

for soil liquid water, and

$$-\rho\varepsilon D_v(\eta_{ws} - \eta_w)\frac{\partial q_s}{\partial z}\bigg|_{z=0} = -E_{dir} + E_0, \quad (25)$$

for water vapor in the soil, respectively, where P_r is the precipitation (kg m^{-2} s^{-1}) and E_r is the surface runoff (kg m^{-2} s^{-1}). The water vapor flux from the pores with adsorbed water film to the atmosphere is E_0 (kg m^{-2} s^{-1}) and expressed by

$$E_0 = \rho(1 - \sigma)c_{E0}|\mathbf{u}|(q_{s0} - q_r), \quad (26)$$

where q_0 is the specific humidity at the soil surface (kg kg^{-1}).

d. Comparison with another land surface model

To evaluate the performance of mod-SOLVEG, comparisons with Noah LSM were carried out. The comparisons of physical processes between mod-SOLVEG and Noah LSM are summarized in Table 2. The prognostic equations of Noah LSM for soil temperature and liquid soil water are basically the same as Eqs. (2) and (3), respectively, except for the evaporation terms. Evaporation is assumed to occur directly from the top shallow soil layer. The direct evaporation (E_{dir}) in mod-SOLVEG is computed by

$$E_{dir} = \beta c_{E0}|\mathbf{u}|[q_{sat}(T_{s0}) - q_r], \quad (27)$$

where β is the evaporation efficiency ranging from 0 to 1. Evaporation efficiency β is determined by a simple linear method (Mahfouf and Noilhan 1991)

$$\beta = \frac{\eta_w - \eta_{wilt}}{\eta_{ref} - \eta_{wilt}}, \quad (28)$$

where η_{ref} and η_{wilt} are the field capacity and the wilting point (m^3 m^{-3}). The change of β for sandy loam soil in Table 1 (Cosby et al. 1984) is depicted in Fig. 4b. This indicates that the change of σ is similar to that of β. In mod-SOLVEG, however, evaporation in the soil by Eq. (18) also contributes to water vapor flux in the dry soil. The mod-SOLVEG therefore continued computing evaporation flux in the dry soil, while Noah LSM ceased computing direct evaporation when the soil water content reached the wilting point.

e. Model parameters and simulation conditions

Values of atmospheric and soil parameters used in this study are provided in Table 3. To calculate the sensible and latent heat fluxes in mod-SOLVEG, the roughness lengths for momentum (z_0) and for heat and water vapor (z_t) are required. The length z_0 is derived

TABLE 3. Model parameters used in the simulation of Negev Desert.

Item	Unit	Value	References
Roughness length			
for momemtum	mm	1.5	In this study
for heat and water vapor	mm	0.2	In this study
Atmospheric pressure	hPa	970	Agam (Ninari) and Berliner (2006)
Precipitation	mm	0	Agam (Ninari) and Berliner (2004)
Albedo	%	37	Qin et al. (2002)
Clay fraction	%	13	Agam (Ninari) and Berliner (2004)
Dry bulk density	kg m^{-3}	1.45	Agam (Ninari) and Berliner (2004)
Porosity	m^{-3} m^{-3}	0.45	Agam (Ninari) and Berliner (2004)
Parameters for thermal conductivity			
A	—	0.78	De Vries (1963)
B	—	1.537	De Vries (1963)
C	—	0.24	De Vries (1963)
D	—	8.354	De Vries (1963)
E	—	4	De Vries (1963)
Parameters for pore model			
κ	—	5.0×10^{-1}	In this study
Hamakar constant	J	-6.0×10^{-20}	Or and Tuller (1999)

from the data of mean wind speed and friction velocity data measured at a single level using the method of Chen et al. (1991). The technique has been applied to determine z_0 for the gravel desert in China and has resulted in a good agreement with the value derived from wind profiles. Only observations corresponding to a bulk Richardson number near zero ($|R_{ib}| < 0.01$) were used for the estimation of z_0 (187 values). Many published studies found that z_t commonly ranged from one-tenth to a third of z_0 in bare soils (Braud et al. 1993). In this study, z_t was assumed to be one-tenth of z_0.

We used the soil thermal conductivity (λ) by McInnes (1981)

$$\lambda = A + B\eta_w - (A - C)\exp[-(D\eta_w)^E], \quad (29)$$

where A, B, C, D, and E are constants derived from De Vries (1963). The specific heat, C_s and density of the soil material, ρ_s, are expressed as (Brutsaert 1982)

$$C_s\rho_s = (1.095 + 4.18\eta_w) \times 10^6. \quad (30)$$

The soil water retention curve for the calculation of evaporation in the soil was not observed at the Negev Desert. Sensitivity tests were thus carried out to evaluate the influence of uncertainty in this parameter. Since many researchers have found a strong relationship between this curve and clay content, m_c (e.g., Banin and Amiel 1970; Petersen et al. 1996; Theng et al. 1999), we compared the Negev soil (m_c = 13%) with two soils called Pachappa loam (m_c = 8.5%) and Yolo silt loam (m_c = 18%). From the relationship of m_c of the three soils, we assumed that the curve for the Negev Desert is almost midway between Pachappa loam and Yolo silt loam. Three soil water retention curves and soil water contents at the 10-mm topsoil layer and calculations using these curves and measurements are shown in Fig. 5a. The parameters of the three soils related to the soil retention curve are given in Table 1. The calculated soil water content using the curve estimated for the Negev Desert is in good agreement with observations (Fig. 5b) considering observational errors and the spatial variability of the soil properties. We therefore use the estimated curve for the model validation.

The upper boundary conditions of Eqs. (2), (3), and (5)—incoming short- and longwave radiation, precipitation, air temperature, wind speed, and specific humidity at the 1-m level above the surface—are prescribed. In mod-SOLVEG, sensible and latent heat fluxes for the atmospheric surface layer are determined by combining the bulk method based on the Monin–Obukov similarity theory. Observed values of T_s and η_w were used for initial conditions of the simulations. Initial values of T_s and η_w deeper than 100 mm were assumed to be uniformly equal to those at 100-mm depth. The specific humidity q_s in the soil pores was prescribed by Eq. (21) for initial and lower boundary conditions. The integration of Eqs. (2), (3), and (5) is performed with a time step of Δt = 3 s. In addition to a single atmospheric layer (1-m level), the grid points in the soil are 0, 0.002, 0.005, 0.01, 0.02, 0.04, 0.1, 0.2, 0.4, 0.65, 0.8, 1.0, 1.15, 1.3, 1.4, and 1.5 m for mod-SOVLEG and 0, 0.1, 0.3, 0.6, 1.0, and 1.5 m for Noah LSM, respectively.

4. Model validation

Simulations by mod-SOLVEG and Noah LSM using measured data from the Negev Desert were carried out.

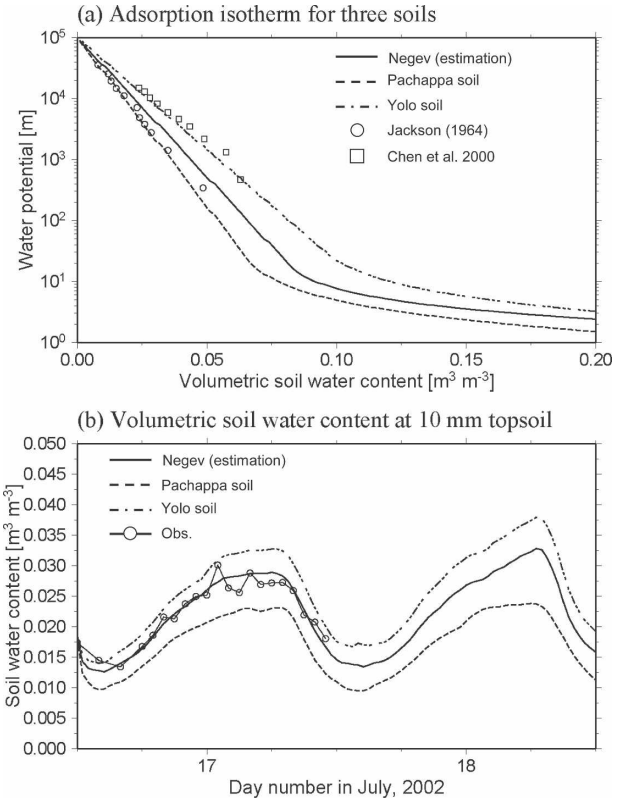

FIG. 5. (a) Soil water retention curves of three soils (solid lines: Negev soil; dashed lines: Pachappa soil; chain lines: Yolo soil; open circles and squares: measurements) and (b) measurements and calculations using the curves from (a) of soil water content from the 10-mm topsoil in the Negev Desert. The curve of Negev is determined to be almost midway between the other two curves.

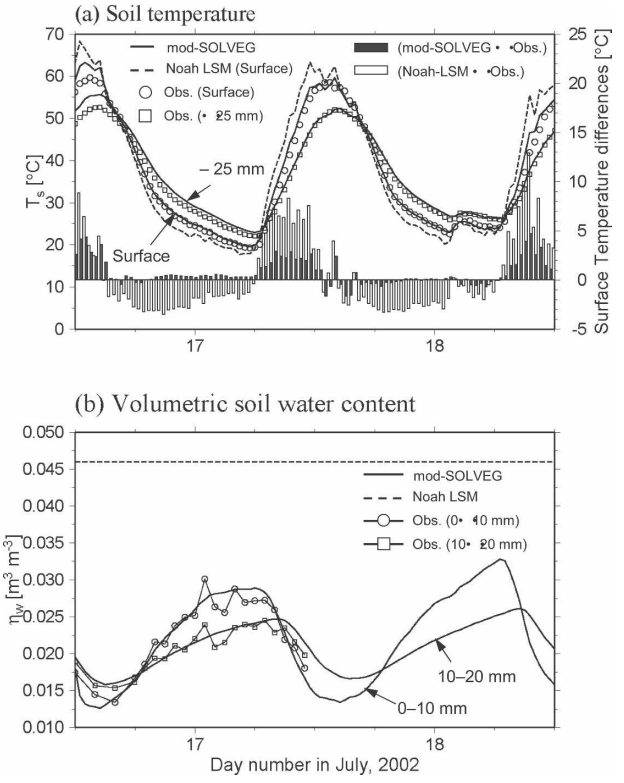

FIG. 6. Temporal changes of (a) soil temperature at the ground surface and at a depth of 25 mm, (b) soil water content of 10–20- and 20–30-mm soil layers from the ground surface in the Negev Desert during the dry season of 2002 (solid lines: calculations by mod-SOLVEG; dashed lines: calculations by Noah LSM; open circles: observations). The bars represent temperature differences (calculations − observations) followed by a right-hand scale.

The outputs were compared with measurements during the dry season from 16 June to 31 October in 2002. Data from 9 to 29 August were not available. Net radiation and soil surface temperature measurements were compared with the model simulations throughout the entire period. During nine 24-h field campaigns, predicted soil water is constant, and sensible and latent heat fluxes were also compared with measurements. Note that the local standard time (UTC + 3) was used for the simulation.

The time series of soil temperatures at the soil surface and at a depth of 25 mm from 17 to 18 July are shown in Fig. 6a. The differences between measurements and calculations are also depicted as a bar graph. Diurnal changes of soil temperatures in mod-SOLVEG agreed with measurements. In contrast, calculations of soil surface temperature by Noah LSM overestimated measurements up to 8°C during the daytime and underestimated them by 3.5°C during the nighttime. The 5° and 3.5°C differences between both models may have been caused by differences in model parameterizations or parameters. However, it is more likely that, to a large extent, these differences have originated from the inherent difference in latent heat flux estimations made by the two models. These differences have a large influence on the heat budget at the soil surface. In another test case using mod-SOLVEG with coarse grid points (0, 0.1, 0.2, 0.4, 0.65, 0.8, 1.0, 1.15, 1.3, 1.4, and 1.5 m), predictions of soil temperature were close to calculations by Noah LSM and calculations of latent heat flux were almost zero (not shown). This indicates that, for accurate predictions of the adsorption process, it is important to use high spatial resolution above a depth of 0.1 m.

Figure 6b shows the time series of the volumetric soil water content at the 10-mm topsoil and the 10–20-mm soil layer. Only the uppermost 100-mm soil layer predicted by Noah LSM was compared. No diurnal variation of soil water was detected by the Noah LSM calculations. This is due to the fact that direct evaporation in Noah LSM does not occur for soil water content that is less than the wilting point (0.047 m^3 m^{-3}). Mod-

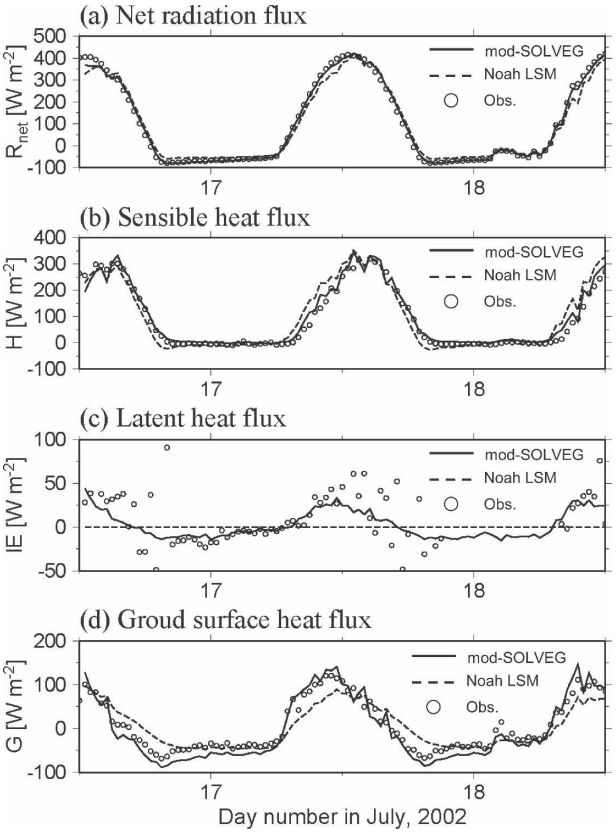

FIG. 7. Temporal changes of (a) net radiation, (b) sensible, (c) latent, and (d) soil heat fluxes in the Negev Desert during the dry season of 2002 (solid lines: calculations by mod-SOLVEG; dashed lines: calculations by Noah LSM; open circles: observations).

SOLVEG, however, predicted the diurnal variation in soil water content ranging from 0.015 to 0.03 m^3 m^{-3} at the 10-mm topsoil, which agrees with observations. This indicates that the newly incorporated processes improved the calculation of soil water.

Temporal changes in net radiation, sensible, latent, and soil heat fluxes are shown in Fig. 7. Mod-SOLVEG predicted the diurnal variations in the measured heat fluxes well. Its prediction of latent heat flux agreed well with measurements, particularly during nighttime. In contrast, in addition to the disagreement between Noah LSM measurements and predictions for sensible and soil heat fluxes, latent heat flux calculated by Noah LSM is zero during both the daytime and nighttime. This is due to the fact that, as mentioned above, soil water content was evidently less than the wilting point.

Figure 8 summarizes the comparison of mod-SOLVEG results with the observations for net radiation, sensible, latent, and soil heat fluxes, soil surface temperature, and soil water content of 10-mm topsoil, during the whole simulation period. For sensible, latent, and soil heat fluxes and soil water content, the comparisons were carried out only during the nine campaigns. The slopes and intercepts of the regression line of the scatterplot of calculations versus observations for all items are close to one and have a very small value, respectively. In particular, modeled and measured values of net radiation and soil surface temperature agreed completely. These results indicate that mod-SOLVEG can provide accurate predictions of surface heat fluxes, soil temperature, and soil water content.

5. Impacts of evaporation and adsorption on water and heat exchanges at the air–land interface

Since the performance of mod-SOLVEG was confirmed in the validation, we used it to carry out numerical experiments along with the standard Noah LSM to evaluate the effects of evaporation and adsorption processes on water and heat exchanges between the air and the soil surface. The initial soil water content was set to 0.2 m^3 m^{-3} for all soil layers. The experiments were performed for a period of 120 days using meteorological data from September to October 2002 at the Negev Desert.

Computations of latent heat flux, soil water content at the uppermost soil layer during first 30 days, and cumulative evaporation and adsorption for 120 days are shown in Fig. 9. These simulations show that after 8 days the soil water content and latent heat flux predicted by Noah LSM remained at wilting point and zero, respectively. This indicates that direct evaporation in Noah LSM at the soil surface stopped when soil water content reached wilting point on day 8. The direct evaporation calculated by mod-SOLVEG dropped almost to zero on day 6. However, it kept simulating small diurnal changes in the latent heat flux and soil water content after 8 days. The decrease of soil water after 8 days was mainly due to evaporation in the soil. On day 120, cumulative evaporation depicted by mod-SOLVEG reaches 69 mm, 46 mm more than that of Noah LSM. The results show that, without considering the adsorption process that balances the amount of water loss due to evaporation, mesoscale models significantly underestimate cumulative evaporation during the drying period because the process of evaporation in the soil is not included in the model.

Until day 20, cumulative adsorption or condensation is almost zero; nonetheless, an apparent increase of soil water during the nighttime is seen (Fig. 9c). The increases of soil water during the nighttime can be explained by the capillary rise of soil water from the USL through the DSL to the soil–atmosphere interface. After 20 days, the DSL reached a thickness of 15 mm and was thick enough to result in a continuous increase in

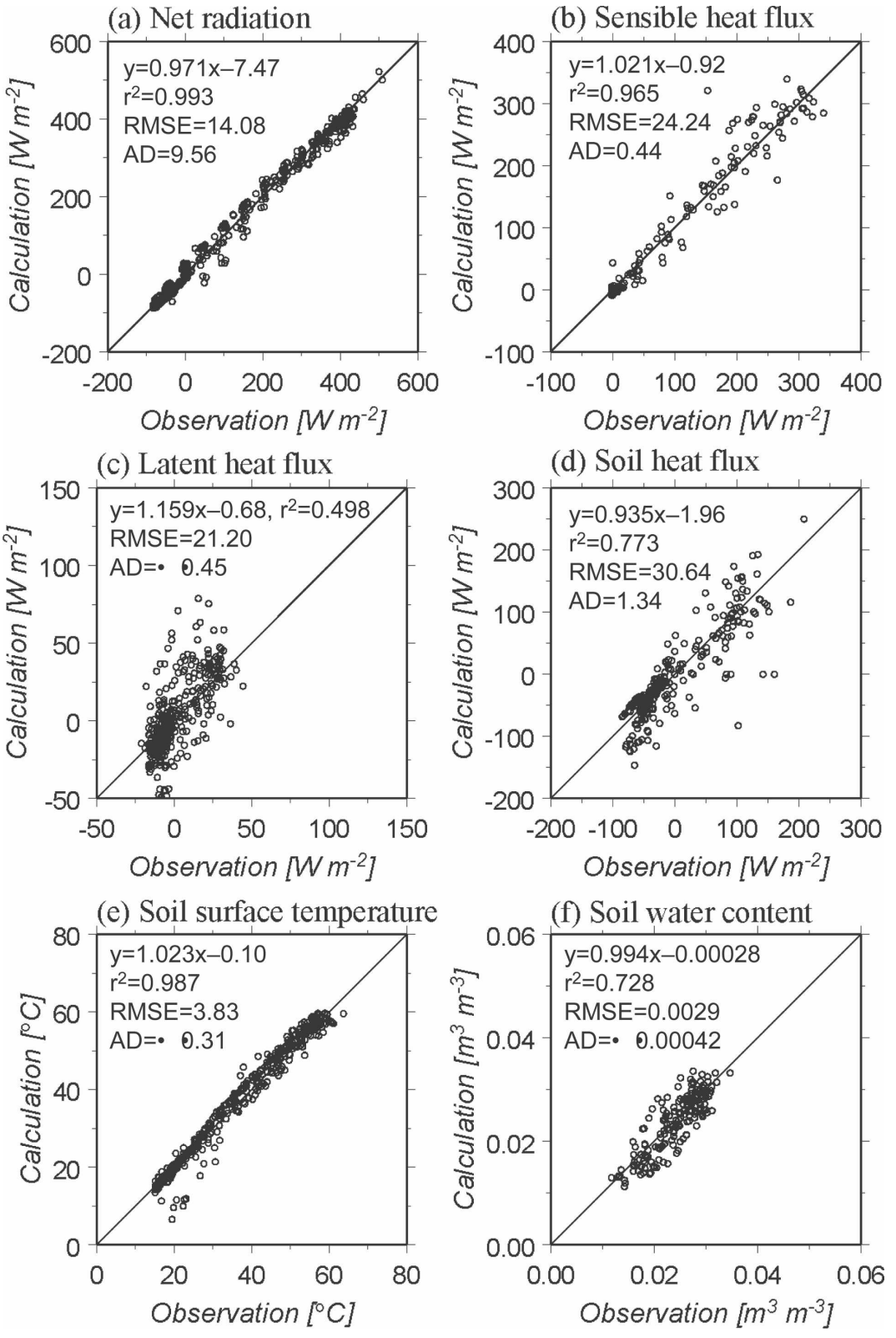

FIG. 8. Comparisons of (a) net radiation, (b) sensible, (c) latent, and (d) soil heat fluxes; (e) soil surface temperature; and (f) soil water content of a 10–20-mm soil layer from the ground surface between the calculated and measured values for the model test period. Statistics are the determination coefficient (r^2), root-mean-square error (RMSE), average difference (AD) [Σ(Obs. − Calc.)/number], and slope and intercept of the regression line.

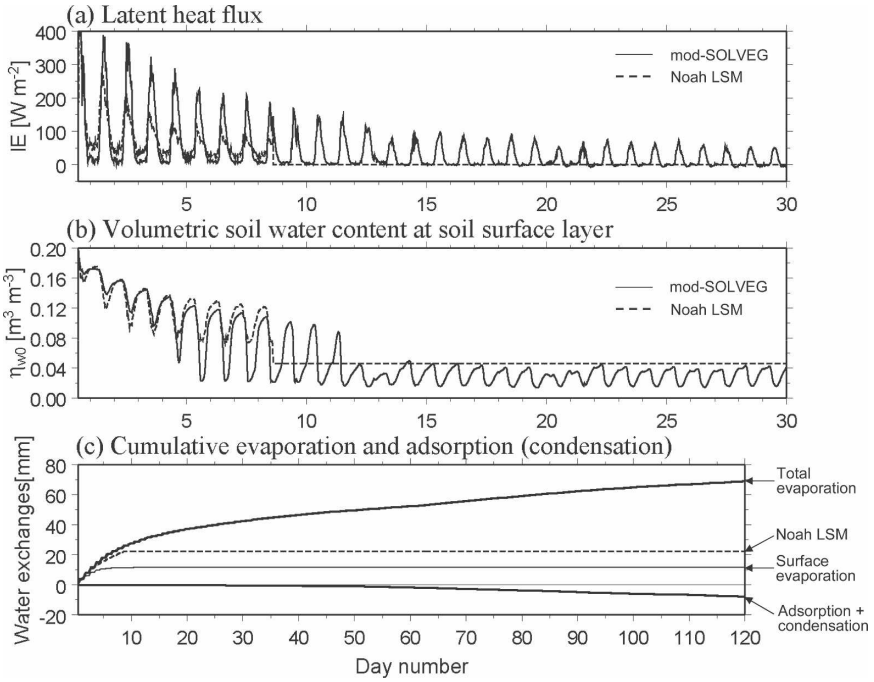

FIG. 9. Temporal changes in the calculations of (a) latent heat flux, (b) volumetric soil water content at the uppermost soil layer, and (c) cumulative evaporation and adsorption (solid lines: calculations by mod-SOLVEG; dashed lines: calculations by Noah LSM). The thin lines in (c) represent direct evaporation calculated by mod-SOLVEG.

the cumulative adsorption. In this condition, condensation of water vapor rarely occurred and the amount of adsorption per night increased with the growth of the DSL. Total adsorption of water at the end of the simulation was 8 mm and was equivalent to 27% of the increase in the cumulative evaporation after 20 days (30 mm). This indicates that the process of adsorption significantly contributed to the water exchange at the air–land interface once the DSL was formed.

After Noah LSM's simulation of direct evaporation dropped to zero, mod-SOLVEG's simulated daily maximum latent heat flux remained in the range of 50 to 150 W m^{-2} $month^{-1}$ (Fig. 9a). Net radiation and sensible heat flux then ranged from 300 to 400 and from 100 to 200 W m^{-2}, respectively. The magnitude of latent heat flux, thus, ranged from one-sixth to half of the net radiation, although direct evaporation at the soil surface had already stopped. To assess the significance of latent heat flux in the energy balance, its magnitude was compared with those of sensible and soil heat fluxes for some soil drying levels (Fig. 10). Latent heat flux occupies 40% to 60% of net radiation during the midday period on day 5 (Fig. 10a), which is larger than the sensible heat flux. Although sensible heat flux turns out to be negative during the night, latent heat flux remained positive and had almost the same magnitude as sensible heat flux. On days 10 and 25, although latent heat flux gradually decreased and sensible flux increased with drying, latent heat flux remained approximately 30% and 20% of net radiation, respectively, which is from 50% to 80% of the sensible heat flux (Figs. 10b,c). This result shows that latent heat flux due to evaporation in the soil significantly affects the energy balance at the soil surface during the drying period.

Although upward latent heat flux during the daytime decreased with further drying (Figs. 10d,e,f), the magnitude of this flux was kept at ~10% of the net radiation (Fig. 10f). Meanwhile, downward latent heat flux due to adsorption in the soil appeared during the nighttime. The magnitude of this downward flux increased with time and became 20% of the net radiation on day 117 (Fig. 10f). Evidence that adsorption increases when the soil dries out has also been found in field investigation (Verhoef et al. 2006). It can be seen that upward latent heat flux during the daytime is due to evaporation of accumulated soil water of this downward latent heat flux during the nighttime.

Comparing the above numerical experiments with the observations at the Negev Desert, it appears that the DSL has been sufficiently developed during the Negev experiment period. The conditions of the Negev experiment are, hence, considered to be situated in the

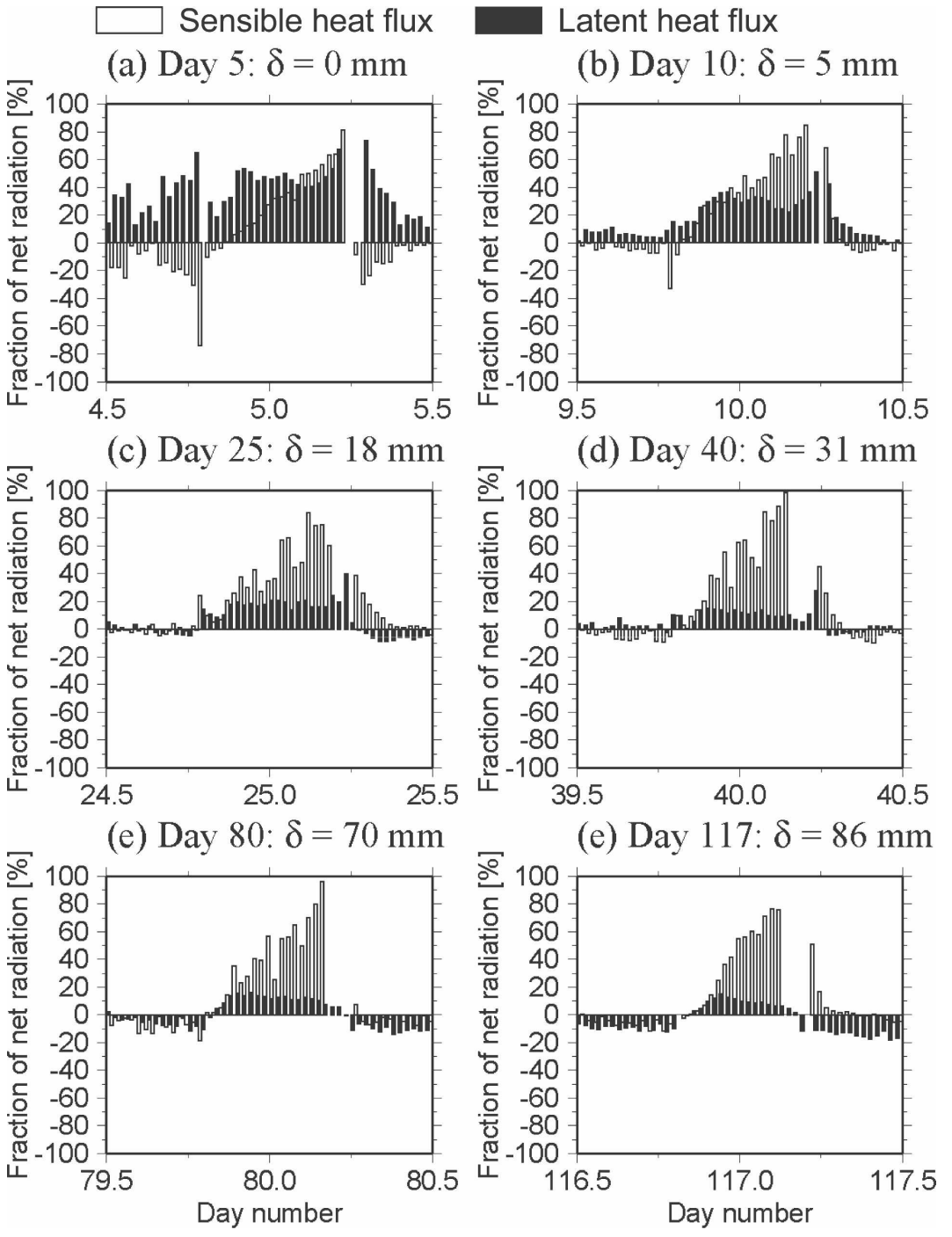

FIG. 10. The relative densities of sensible and latent heat flux as absolute values of the net radiation calculated by mod-SOLVEG on (a) day 5, (b) day 10, (c) day 25, (d) day 40, (e) day 80, and (f) day 117 from the beginning of calculation. Note that δ is a thickness of the DSL.

final stage of the drying period. We investigated water exchange between the air and soil surface in this case using mod-SOLVEG. The simulation was carried out during the entire observation period at the Negev Desert. The simulation parameters used in the experiment were the same as in section 4. Table 4 summarizes the computations of cumulative evaporation and adsorption in the Negev Desert. The difference between evaporation and adsorption was 0.5 to 1 mm month^{-1}. Estimated total evaporation during the daytime and ad-

TABLE 4. Calculations of cumulative evaporation and adsorption using the mod-SOLVEG in the Negev Desert in 2002.

Date in 2002	Evaporation (mm)	Adsorption (condensation) (mm)	Differences (mm)
16–30 Jun	3.83	2.87	0.96
Jul	7.89	6.31	1.57
1–8, 30–31 Aug	2.46	1.93	0.53
Sep	6.17	5.42	0.75
Oct	4.76	4.56	0.20
Total	25.10	21.10	4.00

sorption during the nighttime in the dry season were 25 and 21 mm, respectively, with a difference of 4 mm. Considering some errors caused by model input data—for example, the variation of observed soil water content—this difference is not significant. This indicates that water vapor incoming from the air and outgoing from the soil at the soil surface in the Negev Desert was balanced throughout the experimental periods. In this case, soil surface temperature decreased by the latent heat of evaporation during the daytime and increased by the latent heat of adsorption during the nighttime in the soil, which was compared to the calculations without evaporation and adsorption in the soil (section 4); in other words, the diurnal variation of surface temperature is reduced by the processes of evaporation and adsorption in the soil under dry conditions. This indicates that these processes play an important role not only in the water exchange at the air–land interface but also in reducing the diurnal variation of surface temperature.

6. Conclusions

This paper addressed evaporation and adsorption processes in the soil. A detailed one-dimensional soil model including these processes (mod-SOLVEG) was developed. Simulations by mod-SOLVEG and the Noah Land Surface Model (LSM) implemented in the fifth-generation Penn State–NCAR Mesoscale Model (MM5) were carried out to compare their ability to predict water content, soil temperature, and surface fluxes in the Negev Desert during the dry season. The results revealed that the modifications, which include a new scheme for evaporation and adsorption in the soil, provide good predictions of surface fluxes, soil temperature, and soil water. Mod-SOLVEG reproduced diurnal changes of latent heat flux under dry conditions, which is assumed to be negligible in most of the commonly used models. As a result, a diurnal change of soil water content below the wilting point was depicted by the model computations. The overall performance of mod-SOLVEG for predicting water and heat exchanges at the air–land interface was validated in the dry soil.

Numerical experiments using mod-SOLVEG and Noah LSM were performed to study the impact of the detailed calculations of evaporation and adsorption in the soil on water and heat exchanges at the air–land interface. When the DSL started to develop, evaporation in the soil was a dominant process of water exchange at the air–land interface, while evaporation also occurred at the soil surface. With developing DSL, the adsorption process played a crucial role in the water balance at the soil surface. The upward water vapor flux during daytime was due to evaporation of stored soil water from the downward flux during the nighttime due to the adsorption process. These latent heat fluxes significantly affect the energy balance at the soil surface. Note that when the DSL progressed sufficiently, water adsorption in the soil during the night and evaporation in the soil during the day balanced each other on a monthly basis. Furthermore, the processes of evaporation and adsorption in the soil also work to reduce the diurnal variation in surface temperature.

Acknowledgments. The authors are grateful to Drs. I. Tamagawa, H. Ishikawa, T. Hayashi, M. Horiguchi, J. Wang, Y. Ma, O. Tsukamoto, Hideyuki Nagai, T. Kobayashi, T. Yamanaka, E. Shimojima, K. Sahashi, H. Fujimaki, G. Shinkichi, and T. Kuwagata for their helpful discussion and criticism. We also thank all reviewers for their comments and suggestions. The present study was supported by the Research Revolution Plan 2002 (RR 2002) of the Ministry of Education, Culture, Sports, Science, and Technology.

REFERENCES

Agam (Ninari), N., and P. R. Berliner, 2004: Diurnal water content changes in the bare soil of a coastal desert. *J. Hydrometeor.,* **5,** 922–933.

——, and ——, 2006: Dew formation and water vapor adsorption in semi-arid environments—A review. *J. Arid Environ.,* **65,** 572–590.

——, ——, A. Zangvil, and E. Ben Dor, 2004: Soil water evaporation during the dry season in an arid zone. *J. Geophys. Res.,* **109,** D16103, doi:10.1029/2004JD004802.

Anwar, A. H. M. F., T. H. Tien, Y. Inoue, and F. Takagi, 2003: Mass transfer correlation for nonaqueous phase liquid volatilization in porous media. *Environ. Sci. Technol.,* **37,** 1277–1283.

Banin, A., and A. Amiel, 1970: A correlative study of the chemical and physical properties of a group of natural soils of Israel. *Geoderma,* **3,** 185–198.

Barrett, E. P., L. G. Joyner, and P. P. Halenda, 1951: The determination of pore volume and area distributions in porous

substances. I. Computations from nitrogen isotherms. *J. Amer. Chem. Soc.,* **73,** 373–380.

Bird, R. B., W. E. Stewart, and E. N. Lightfoot, 2001: *Transport Phenomena*. Wiley, 920 pp.

Blunt, M. J., and H. Scher, 1995: Pore-level modeling of wetting. *Phys. Rev. E,* **52,** 6387–6403.

Bougeault, P., 1991: Parameterization schemes of land-surface processes for mesoscale atmospheric models. *Land Surface Land Surface Evaporation: Measurement and Parameterization,* T. J. Schmugge and J.-C. Andre, Eds., Springer, 55–92.

Braud, I., J. Noilhan, P. Bessemoulin, P. Mascart, R. Haverkamp, and M. Vauclin, 1993: Bare-ground surface heat and water exchanges under dry conditions: Observations and parameterization. *Bound.-Layer Meteor.,* **66,** 173–200.

Brooks, R. H., and A. T. Corey, 1964: Hydraulic properties of porous media. Hydrology Paper 3, Colorado State University, Fort Collins, 27 pp.

Brunauer, S., P. H. Emmett, and E. Teller, 1938: Adsorption of gases in multimolecular layers. *J. Amer. Chem. Soc.,* **60,** 309–319.

Brutsaert, W., 1982: *Evaporation into the Atmosphere*. D. Reidel, 299 pp.

Cahill, A. T., and M. B. Parlange, 1998: On water transport in field soils. *Water Resour. Res.,* **34,** 731–739.

Campbell, G. S., and S. Shiozawa, 1992: Prediction of hydraulic properties of soils using particle size distribution and bulk density data. *International Workshop on Indirect Methods for Estimating the Hydraulic Properties of Unsaturated Soils,* University of California, 317–328.

Chen, D., D. E. Rolston, and T. Yamaguchi, 2000: Calculating partition coefficients of organic vapors in unsaturated soil and clays. *Soil Sci.,* **165,** 217–225.

Chen, F., and J. Dudhia, 2001a: Coupling an advanced land surface–hydrology model with the Penn State–NCAR MM5 modeling system. Part I: Model implementation and sensitivity. *Mon. Wea. Rev.,* **129,** 569–585.

——, and ——, 2001b: Coupling an advanced land surface–hydrology model with the Penn State–NCAR MM5 modeling system. Part II: Preliminary model validation. *Mon. Wea. Rev.,* **129,** 587–604.

Chen, J. Y., J. M. Wang, and Y. Mitsuta, 1991: An independent method to determine the surface roughness parameter. *Bull. Disas. Prev. Res. Inst. Kyoto Univ.,* **41,** 121–127.

Cleugh, H. A., and T. Roberts, 1994: Local-scale energy balances and microclimate in the desert ranges of central Australia. *Aust. Meteor. Mag.,* **43,** 219–228.

Cosby, B. J., G. M. Hornberger, R. B. Glapp, and T. R. Ginn, 1984: A statistical exploration of the relationships of soil moisture characteristics to the physical properties of soils. *Water Resour. Res.,* **20,** 682–690.

Cranston, R. W., and F. A. Inkley, 1957: The determination of pore structures from nitrogen adsorption isotherms. *Adv. Catal.,* **9,** 143–154.

Derjaguin, B. V., N. V. Churaev, and V. M. Muller, 1987: *Surface Forces*. Consultants Bureau, 440 pp. [Translated from Russian by V. I. Kisin.]

De Vries, D. A., 1963: Thermal properties of soils. *Physics of Plant Environment,* W. R. van Wijk, Ed., North Holland Publishing, 210–235.

——, 1987: The theory of heat and moisture transfer in porous media revisited. *Int. J. Heat Mass Transfer,* **30,** 1343–1350.

Dollimore, D., and G. R. Heal, 1964: An improved method for the calculation of pore size distribution from adsorption data. *J. Appl. Chem.,* **14,** 109–114.

Grifoll, J., J. Ma. Gasto, and Y. Cohen, 2005: Non-isothermal soil water transport and evaporation. *Adv. Water Resour.,* **28,** 1254–1266.

Hillel, D., 1998: *Environmental Soil Physics*. Academic Press, 757 pp.

Israelachvili, J. N., 1992: *Intermolecular and Surface Forces.* 2d ed. Academic Press, 45 pp.

Iwamatsu, M., and K. Horii, 1996: Capillary condensation and adhesion of two wetter surfaces. *J. Colloid Interf. Sci.,* **182,** 400–406.

Jackson, R. D., 1964: Water vapor diffusion in relatively dry soil: III. Steady-state experiments. *Soil Sci. Soc. Amer. Proc.,* **28,** 467–470.

——, R. J. Reginato, B. A. Kimball, and F. S. Nakayama, 1974: Diurnal soil-water evaporation: Comparison of measured and calculated soil-water fluxes. *Soil Sci. Soc. Amer. Proc.,* **38,** 861–866.

Kim, H., P. S. C. Rao, and M. D. Annable, 1997: Determination of effective air-water interfacial area in partially saturated porous media using surfactant adsorption. *Water Resour. Res.,* **33,** 2705–2711.

Kosugi, K., 1994: Three-parameter lognormal distribution model for soil water retention. *Water Resour. Res.,* **30,** 891–901.

Mahfouf, J. F., and J. Noilhan, 1991: Comparative study of various formulations of evaporation from bare soil using in situ data. *J. Appl. Meteor.,* **30,** 1354–1365.

McInnes, K., 1981: Thermal conductivities of soils from dryland wheat regions in eastern Washington. M.S. thesis, Dept. of Agronomy and Soils, Washington State University, 51 pp. [Available from Owen Science Library, Washington State University, Pullman, WA 99163-3200.]

Milly, P. C. D., 1982: Moisture and heat transport in hysteretic, inhomogeneous porous media: A matric head-based formulation and a numerical model. *Water Resour. Res.,* **18,** 489–498.

Mualem, Y., 1976: New model for predicting the hydraulic conductivity of unsaturated porous media. *Water Resour. Res.,* **12,** 513–522.

Nagai, H., 2002: Validation and sensitivity analysis of a new atmosphere–soil–vegetation model. *J. Appl. Meteor.,* **41,** 160–176.

——, 2003: Validation and sensitivity analysis of a new atmosphere–soil–vegetation model. Part II: Impacts on in-canopy latent heat flux over a winter wheat field determined by detailed calculation of canopy radiation transmission and stomatal resistance. *J. Appl. Meteor.,* **42,** 434–451.

——, 2005: Incorporation of CO_2 exchange processes into a multilayer atmosphere–soil–vegetation model. *J. Appl. Meteor.,* **44,** 1574–1592.

——, and H. Yamazawa, 1999: Development of One-dimensional Atmosphere-soil-vegetation Model. Rep. 99-024, Japan Atomic Energy Research Institute, 88 pp.

Ninari, N., and P. R. Berliner, 2002: The role of dew in the water and heat balance of bare loess soil in the Negev Desert: Quantifying the actual dew deposition on the soil surface. *Atmos. Res.,* **64,** 323–334.

Or, D., and M. Tuller, 1999: Liquid retention and interfacial area in variably saturated porous media: Upscaling from single-pore to sample-scale model. *Water Resour. Res.,* **35,** 3591–3605.

Petersen, L. W., P. Moldrup, O. H. Jacobsen, and D. E. Rolston,

1996: Relations between specific surface area and soil physical and chemical properties. *Soil Sci.,* **161,** 9–20.

Philip, J. R., and D. A. De Vries, 1957: Moisture movement in porous materials under temperature gradients. *Trans. Amer. Geophys. Union,* **38,** 222–232.

Puigdefabregas, J., 1995: Desertification: Stress beyond resilience, exploring a unifying process structure. *Ambio,* **24,** 311–313.

Qin, Z., P. Berliner, and A. Karnieli, 2002: Micrometeorlogical modeling to understand the thermal anomaly in the sand dunes across the Israel-Egypt border. *J. Arid Environ.,* **51,** 281–318.

Ransohoff, T. C., and C. J. Radke, 1988: Laminar flow of a wetting liquid along the corners of a predominantly gas-occupied noncircular pore. *J. Colloid Interf. Sci.,* **121,** 392–401.

Reeves, P. C., and M. A. Celia, 1996: A functional relationship between capillary pressure, saturation, and interfacial area as revealed by a pore-scale network model. *Water Resour. Res.,* **32,** 2345–2358.

Rolston, D. E., 1986: Gas flux. *Methods of Soil Analysis, Part 1: Physical and Mineralogical Methods, Monogr.,* No. 9, American Society of Agronomy, 1103–1119.

Rose, D. A., F. Konukcu, and J. W. Gowing, 2005: Effect of watertable depth on evaporation and salt accumulation from saline groundwater. *Aust. J. Soil Res.,* **43,** 565–573.

Shimojima, E., A. A. Curtis, and J. V. Turner, 1990: The mechanism of evaporation from sand columns with restricted and unrestricted water tables using deuterium under turbulent airflow conditions. *J. Hydrol.,* **117,** 15–54.

Sridhar, V., R. L. Elliott, F. Chen, and J. A. Brotzge, 2002: Validation of the NOAH-OSU land surface model using surface flux measurements in Oklahoma. *J. Geophys. Res.,* **107,** 4418, doi:10.1029/2001JD001306.

Theng, B. K. G., G. G. Ristori, C. A. Santi, and H. J. Percival, 1999: An improved method for determining the specific surface areas of topsoils with varied organic matter content, texture and clay mineral composition. *Eur. Soil Sci.,* **50,** 309–316.

Tuller, M., O. Dani, and L. M. Dudley, 1999: Adsorption and capillary condensation in porous media: Liquid retention and interfacial configurations in angular pores. *Water Resour. Res.,* **35,** 1949–1964.

Unland, H. E., P. R. Houser, W. J. Shuttleworth, and Z.-L. Yang, 1996: Surface flux measurement and modeling at a semi-arid Sonoran Desert site. *Agric. For. Meteor.,* **82,** 119–153.

Van Genuchten, M. Th., 1980: Closed-form equation for predicting the hydraulic conductivity of unsaturated soils. *Soil Sci. Soc. Amer. J.,* **44,** 892–898.

Verhoef, A., A. Diaz Espejo, J. R. Knight, L. Villagarcia, and J. E. Fernandez, 2006: Adsorption of water vapor by bare soil in an olive grove in southern Spain. *J. Hydrometeor.,* **7,** 1011–1027.

Verstraete, M. M., and S. A. Schwartz, 1991: Desertification and global change. *Vegetatio,* **91,** 3–13.

Warren, A., 1996: Desertification. *The Physical Geography of Africa,* W. M. Adams, A. S. Goudie, and A. R. Orme, Eds., Oxford University Press, 342–355.

Webb, S. W., 2000: A simple extension of two-phase characteristic curves to include the dry region. *Water Resour. Res.,* **36,** 1425–1430.

Wheeler, A., 1955: Reaction rates and selectivity in catalyst pores. *Catalysis,* **2,** 105–165.

Yamazawa, H., and H. Nagai, 1997: Development of one-dimensional atmosphere-bare soil model. Rep. 97-041, Japan Atomic Energy Research Institute, 56 pp.

Yang, Z.-L., R. E. Dickinson, W. J. Shuttleworth, and M. Shaikh, 1998: Treatment of soil, vegetation and snow in land surface models: A test of the Biosphere-Atmosphere Transfer Scheme with the HAPEX-MOBILHY, ABRACOS and Russian data. *J. Hydrol.,* **212–213,** 109–127.

Zand-Parsa, Sh., and A. R. Sepaskhah, 2004: Soil hydraulic conductivity function based on specific liquid-vapor interfacial area around the soil particles. *Geoderma,* **119,** 143–157.